Available online at www.sciencedirect.com
SCIENCE DIRECT®
Journal of Solid State Chemistry 178 (2005) 2647–2657
JOURNAL OF SOLID STATE CHEMISTRY
www.elsevier.com/locate/jssc

A coupled electron diffraction and rigid unit mode (RUM) study of the crystal chemistry of some zeotypic $AlPO_4$ compounds

Ray L. Withers*, Yun Liu

Research School of Chemistry, Australian National University, Canberra, ACT 0200, Australia

Received 6 May 2005; received in revised form 2 June 2005; accepted 5 June 2005
Available online 14 July 2005

Abstract

Electron diffraction and lattice dynamical calculations are used to investigate the unit cells, space group symmetries and inherent displacive flexibility of the room-temperature average structures of $AlPO_4$-8, $AlPO_4$-16 and $AlPO_4$-tridymite. The zero-frequency rigid unit modes (RUMs) of the idealized high-symmetry polymorphs thereof are also investigated along with their relationship to the lower-temperature polymorphism of these zeotypic aluminophosphates. The clear presence of $\mathbf{G} \pm \frac{1}{2}\mathbf{c}^*$ satellite reflections in addition to the Bragg reflections (**G**) of the underlying $Cmc2_1$ parent structure in the case of $AlPO_4$-8 shows that the true unit cell of the room-temperature polymorph has a doubled *c*-axis due to a condensed RUM mode. Structured diffuse scattering is also observed which can be related to the thermal excitation of RUM modes. In the case of $AlPO_4$-tridymite, a complex *F*1 triclinic polymorph is observed and related to soft RUM modes while, in the case of $AlPO_4$-16, a soft $\mathbf{q} = \mathbf{0}$ RUM mode is shown to be responsible for an observed phase transition in the case of the all SiO_2 analogue of $AlPO_4$-16. A large number of additional zero-frequency RUM modes also exist in the case of $AlPO_4$-16.

Keywords: Microporous aluminophosphates; Characteristic diffuse distributions; Dynamical disorder; Correlated tetrahedral rotations

1. Introduction

The large family of zeotypic, tetrahedrally corner-connected, aluminophosphate framework structures have been intensively investigated ever since they were first discovered [1] as a result of their potential for use in catalysis, ion exchange and as molecular sieve materials [2–5]. Despite the rigidity of their tetrahedral building blocks as well as the fixed nature of their topological connectedness, many such aluminophosphates retain considerable inherent dynamic displacive flexibility [6,7]. This inherent flexibility arises from the often surprisingly large number of ways in which it is possible to change the relative orientation and positioning of neighbouring tetrahedral units without distorting the essentially rigid tetrahedral units themselves [8,9]. It manifests itself in sharp (in at least one local reciprocal space direction), highly structured, continuous diffuse intensity distributions which map out the 'zero-frequency' rigid unit mode (RUM) modes [8–12] characteristic of the particular framework structure. Structured diffuse intensity distributions of this type are most easily visible in electron diffraction patterns (EDPs) and have recently been shown to be characteristic of the room-temperature structures of both $AlPO_4$-5 [6] as well as $AlPO_4$-11 [7].

Conventional average structure refinements of such dynamically disordered framework structures almost invariably lead to chemically unsound crystal structures (with too short metal (*T*)–O distances within constituent tetrahedra, chemically unreasonable linear *T*–O–*T* angles along with large and/or strongly anisotropic thermal parameters [6,7,13,14]) as a result of the fact that the large amplitude excitation of RUM modes is typically ignored in such refinements. When this is the

*Corresponding author. Fax: +61 2 6125 0750.
E-mail address: withers@rsc.anu.edu.au (R.L. Withers).

0022-4596/$ - see front matter © 2005 Elsevier Inc. All rights reserved.
doi:10.1016/j.jssc.2005.06.003

case, it is reflected in calculated bond valence sums, or apparent valences [15], which usually differ strongly from expected ideal valences when the reported average structure fractional co-ordinates are used [6,7]. Such a situation, e.g., occurs in the case of the reported *F*23 average structure refinement of $AlPO_4$-16 [16] where chemically unsound linear Al–O–P angles exist as well as metal–O distances within AlO_4 and PO_4 tetrahedra that are far too short and lead to heavily over-bonded Al, P and O ions (see Table 1). Clearly, this reported average structure does not give a good idea of the instantaneous local structure of $AlPO_4$-16.

One way to avoid such crystal chemically unreasonable resultant crystal structures is to undertake distance least squares (DLS) refinements (see e.g. Ref. [17] where a constrained DLS refinement of the structure of $AlPO_4$-8 has been reported) whereby the Al–O and P–O bond lengths are constrained to be reasonable. For such a refinement to reflect reality, however, it is essential that the appropriate average structure unit cell and space group symmetry is chosen. Otherwise, such a refinement is tantamount to making the assumption that only a very particular RUM mode of distortion (e.g., a $\mathbf{q} = \mathbf{0}$ RUM mode) has frozen in.

Such a situation may well have happened in the case of $AlPO_4$-8 where the DLS determined room-temperature structure of Dessau et al. [17], as well as the subsequent refinement of Poojary and Clearfield [18], used an average structure unit cell and space group symmetry corresponding to the maximum topological symmetry of the $AlPO_4$-8 framework structure. A later neutron powder diffraction study [19] reported the existence of additional superlattice reflections not consistent with this unit cell and space group symmetry at room temperature and below which disappeared on heating to ~200 °C. Neither a supercell nor a space group symmetry for this room-temperature structure, however, were given. These authors [19] also reported the existence of a '…non-crystalline (background) component…' suggestive of the presence of a significant diffuse intensity component co-existing with the strong Bragg reflections of the underlying average structure [7]. Clearly, the room-temperature unit cell and space group symmetry of $AlPO_4$-8 need to be re-examined by a technique more sensitive to weak features of reciprocal space such as electron diffraction [6,7].

Given the existence of numerous potential RUM modes at higher temperatures, it should not be surprising that, on lowering of temperature, many of these dynamically disordered framework structures undergo polymorphic phase transitions involving condensation of one or more RUM modes of distortion. Polymorphic phase transitions of this sort occur, e.g., in the case of the tridymite forms of SiO_2 (see e.g. Refs. [20,21]) and $AlPO_4$ [22–24] as well as in the all silicon analogue of $AlPO_4$-5, SSZ-24 [25], etc. Given the sensitivity of electron diffraction to weak features of reciprocal space difficult to pick up by means of powder diffraction coupled with the absence of such a study in the case of $AlPO_4$-tridymite, it was decided to attempt to fill this gap. The purpose of the current paper then is to present the results of a combined room-temperature electron diffraction and RUM study of the crystal chemistry of the $AlPO_4$ compounds, $AlPO_4$-8, $AlPO_4$-16 and $AlPO_4$-tridymite.

Table 1
Bond valence sums or apparent valences (AVs) calculated from the *F*23 average structure refinement of $AlPO_4$-16 reported in Ref. [16]

Structure	*F*23 [16]	Ideal
Bond valence parameter *R*	Al–O = 1.651 Å	Al–O = 1.7574 Å
	P–O = 1.604 Å	P–O = 1.5214 Å
	O–O = 1.480 Å	O–O = 2.4844 or 2.8698 Å
At Al(1)	2.917	3.000
At Al(2)	***3.342***	
At P(1)	***6.461***	5.000
At P(2)	***6.738***	
At O(1)	2.270	2.000
At O(2)	***2.543***	
At O(3)	***2.544***	

($V = \exp((R-d)/0.37\,\text{Å}$, calculated using the bond valence parameters listed in Ref. [15]). Sites where the calculated AV deviates markedly from the expected ideal AV are highlighted in bold and italicized.

2. Experimental

2.1. Synthesis

2.1.1. Preparation of $AlPO_4$-8, $AlPO_4$-16 and $AlPO_4$-tridymite

The three aluminium phosphates ($AlPO_4$-8, $AlPO_4$-16 and $AlPO_4$-tridymite) were synthesized using a three-step reaction procedure. The first step involved the formation of a gel, the second a hydrothermal treatment of the gel and the third the recovery of the product.

$AlPO_4$-8 powders were obtained from pre-synthesized $AlPO_4$-54, in turn prepared via the following hydrothermal reaction. A reaction mixture was obtained by slowly dropping the appropriate amount of orthophosphoric acid (H_3PO_4, 85 wt%, Univar) into distilled H_2O. A stoichiometric amount of *böhmite* alumina (HIQ-30, Alcoa, 75 wt% Al_2O_3) was then added. This resultant solution was then manually stirred until homogeneous and aged for 2 h with periodic stirring at 20 min intervals. A mixture of *N*-ethylbutylamine (used as a template *R*: $CH_3(CH_2)_3NHC_2H_5$, Aldrich) and distilled H_2O was then added into the aged solution and vigorously stirred. The mixture was then allowed to age

for a further 2 h to form a uniform gel. The nominal composition of this gel in molar ratios was Al_2O_3:-P_2O_5:R:40H_2O and the total volume used in the experiment about 50 mL.

This gel was then put into a 220 mL stainless steel pressure vessel together with 100 mL of H_2O, sealed and heated in an oven at 150 °C at autogenous pressure for 4 h followed by rapid quenching in water. The as-quenched solid product was then recovered by filtration, washed with distilled water and acetone, and dried in air at 50 °C. The resultant product was a crystalline powder. X-ray powder diffraction gave a hexagonal unit cell ($a = 18.953(4)$ Å and $c = 8.101(2)$ Å) in excellent agreement with literature lattice parameters for $AlPO_4$-54 [26,27].

$AlPO_4$-8 was obtained by heat treatment of this $AlPO_4$-54 powder. Fig. 1 shows the differential scanning calorimetry (DSC) curve of $AlPO_4$-54 using a heating rate of 5 °C/min. As can be seen, a large exothermic signal occurs at 155 °C. XRD showed a quite distinct pattern consistent with the reported orthorhombic $Cmc2_1$ structure of $AlPO_4$-8 whenever $AlPO_4$-54 was heated at a temperature higher than 155 °C for 1–5 days followed by quenching into water. $AlPO_4$-54 specimens heat-treated at 160, 200 and 600 °C all transformed into $AlPO_4$-8. No difference could be observed in their XRD patterns, suggesting that the small signal seen in the DSC curve at 348 °C is not related to a structural change. It may be due to desorption of water. The lattice parameters of the $AlPO_4$-8 samples obtained from heat treatment at 200 °C for 5 days were $a = 32.723(12)$ Å, $b = 15.600(7)$ Å, and $c = 8.211(3)$ Å.

AlPO4-16 was prepared using the same starting materials as for $AlPO_4$-54 except for the use of a different template R. In this case, quinclidine ($C_7H_{13}N$, 97%, Aldrich, 1.1463 g) was used. The solution was roughly stirred and hydrofluoric acid (HF) added. The fluoride ions were used as a mineralizing agent for symmetry control in conjunction with the template. The nominal composition for the $AlPO_4$-16 gel was Al_2O_3:R:P_2O_5:60H_2O:HF. The resultant solution was manually stirred until it formed a uniform gel. This gel was then sealed in a teflon-lined stainless steel pressure vessel and heated in an oven at 150 °C at autogenous pressure for 24 h. The vessel was then taken out from the oven and quenched into water. The as-made solid product was recovered by diluting and filtration, washed with distilled water and acetone and then dried in air at 150 °C to remove the water. In this case, the resultant powder (white) was found to be tetragonal with lattice parameters, $a = 9.3590(10)$ Å and $c = 13.4905(18)$ Å, in good agreement with Patarins' result [28]. The organic and fluoride species were removed by heating the sample at 500 °C in air for 2 h. The resultant $AlPO_4$-16 powder had grey colour and a cubic unit cell ($a = 13.479(1)$ Å).

The synthesis of the $AlPO_4$-tridymite was again carried out using the same raw materials as above. The chosen template (R) in this case was triethylamine (TEA, $(C_2H_5)_3N$, 99%, Aldrich). The nominal composition for the $AlPO_4$-tridymite gel was 0.33Al_2O_3:-P_2O_5:1.1R:47H_2O. It is vital when synthesizing $AlPO_4$-tridymite, that the pH value of the solution does not deviate from 5. After mixing the above starting materials to obtain a uniform gel, the resultant pH was found to be 3. Subsequently small amounts of 0.1 N NaOH(aq) were added to adjust the pH to 5 after which the solution was stirred for 1 h. The subsequent hydrothermal reaction was done at 170 °C for 6 h. The as-made solid product was recovered by filtration, washed with distilled water and acetone and dried in air at 50 °C. The resultant power was determined by XRPD to have a unit cell with lattice parameters of $a = 37.401(4)$ Å, $b = 4.988(2)$ Å, $c = 26.026(9)$ Å and $\beta = 118.28(3)$.

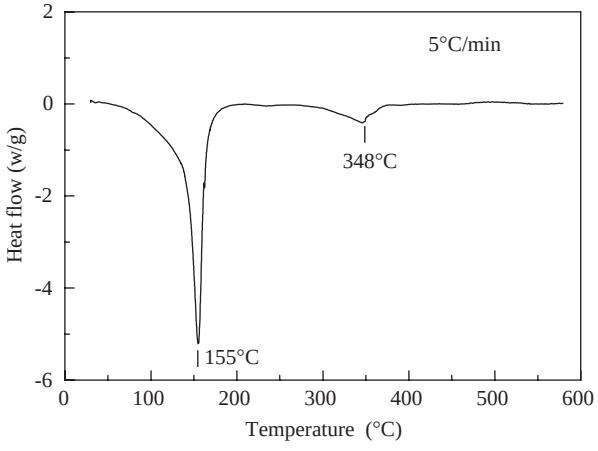

Fig. 1. The differential scanning calorimetry (DSC) curve of $AlPO_4$-54 at a heating rate of 5 °C/min. A large exothermic signal occurs at 155 °C corresponding to the transformation from $AlPO_4$-54 to $AlPO_4$-8. $AlPO_4$-54 specimens heat-treated at 160, 200 and 600 °C all transformed into $AlPO_4$-8. No difference could be observed in their XRD patterns, suggesting that the small signal seen in the DSC curve at 348 °C is not related to a structural change.

2.2. X-ray powder diffraction

The average structure unit cell dimensions of the samples investigated (given above) were determined using a Guinier–Hägg camera. Silicon ($a = 5.431195$ Å at 22.5 °C [29]) was used as an internal standard and the corrected diffraction lines were refined with a least squares program [30].

2.3. Electron diffraction

Crushed specimens were deposited on holey-carbon coated grids and examined in a Philips EM 430 transmission electron microscope operating at 300 kV.

Given the sensitivity of the specimens to electron beam irradiation, electron dose always needed to be minimized as far as possible.

3. Results

3.1. Electron diffraction results

3.1.1. $AlPO_4$-8

Fig. 2 shows (a) $\langle 1\bar{1}0\rangle$, (b) $\langle 3\bar{5}0\rangle$, (c) $\langle 1\bar{3}0\rangle$ and (d) [010] zone axis EDPs typical of the room-temperature form of $AlPO_4$-8 indexed with respect to the parent $Cmc2_1$, $a\sim32.72$, $b\sim15.60$, $c\sim8.21$ Å unit cell. Note the clear presence of $\mathbf{G}\pm\frac{1}{2}\mathbf{c}^*$ satellite reflections in addition to the Bragg reflections (**G**) of the underlying $Cmc2_1$ parent structure. The existence of these additional superlattice reflections is in agreement with the neutron powder diffraction study of Ref. [19] as discussed above, as is the presence of co-existing structured diffuse scattering apparent in more heavily exposed EDPs at some zone axis orientations—see e.g. Fig. 3. The true room-temperature unit cell of $AlPO_4$-8 thus clearly has a doubled c-axis and remains C-centred. This rules out both the $Pmn2_1$, $a\sim34$, $b\sim14.5$, $c\sim8.3$ Å [31,32] as well as the $P2_1$, $a=14.63$, $b=18.1$, $c=8.36$ Å [32] superstructures predicted as possible room-temperature structures of $AlPO_4$-8 using lattice energy minimization techniques [31,32]. It also invalidates the DLS refinement of Ref. [17] as well as the refinement reported in Ref. [18].

Group theoretical considerations [33] suggest that the most likely resultant space group symmetry of the true $a\sim32.72$, $b\sim15.60$, $c\sim2\times8.21$ Å unit cell (given parent $Cmc2_1$ space group symmetry) is monoclinic $Cm11$ or $Cc11$. In principle, these would be easy to distinguish if only a [100] zone axis EDP could be obtained. Unfortunately, the morphology of the crushed samples in conjunction with the extreme beam sensitivity of $AlPO_4$-8 has made this a near impossible task. Crushed crystalline fragments of the as-prepared $AlPO_4$-8 specimens invariably possess a very platey morphology with the normal to the plate corresponding to the crystallographic **b**-axis so that by far the most commonly obtained major zone axis orientation observed was [010] (see Fig. 2d). Unfortunately, $AlPO_4$-8 was also found to be rather beam sensitive so that only one or at most two EDPs could be obtained before that particular grain 'died'. This makes systematic tilting experiments nigh on impossible.

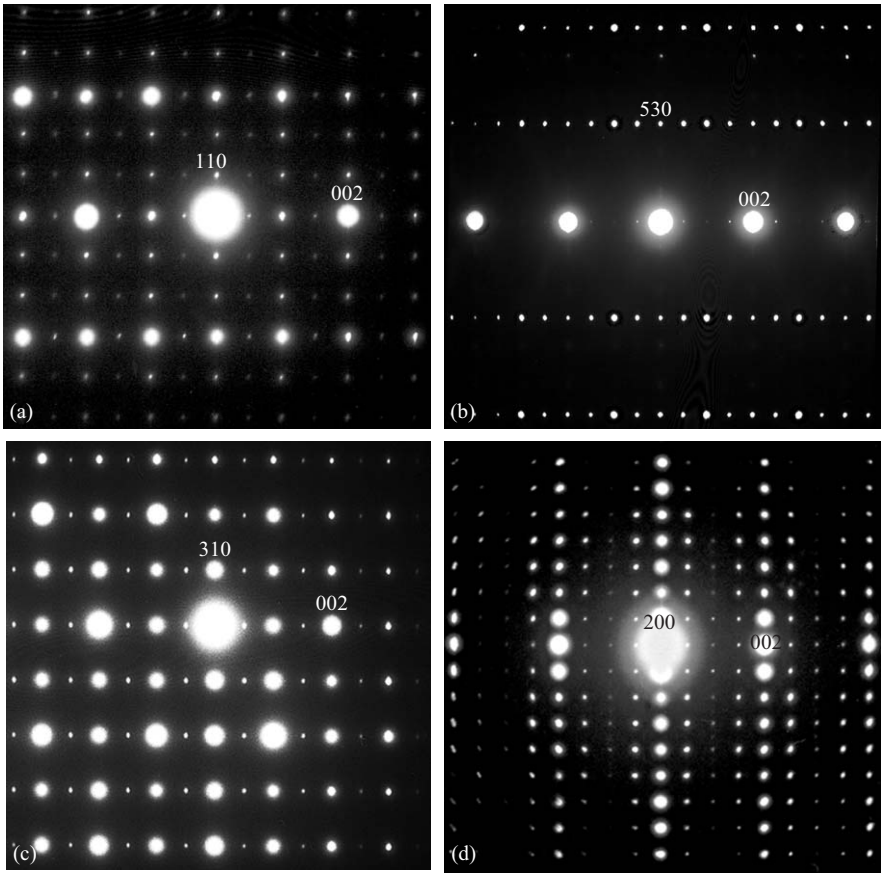

Fig. 2. (a) $\langle 1\bar{1}0\rangle$, (b) $\langle 3\bar{5}0\rangle$, (c) $\langle 1\bar{3}0\rangle$ and (d) [010] zone axis EDPs typical of the room-temperature form of $AlPO_4$-8 indexed with respect to the parent $Cmc2_1$, $a\sim32.72$, $b\sim15.60$, $c\sim8.21$ Å unit cell. Notice the clear presence of $\mathbf{G}\pm\frac{1}{2}\mathbf{c}^*$ satellite reflections.

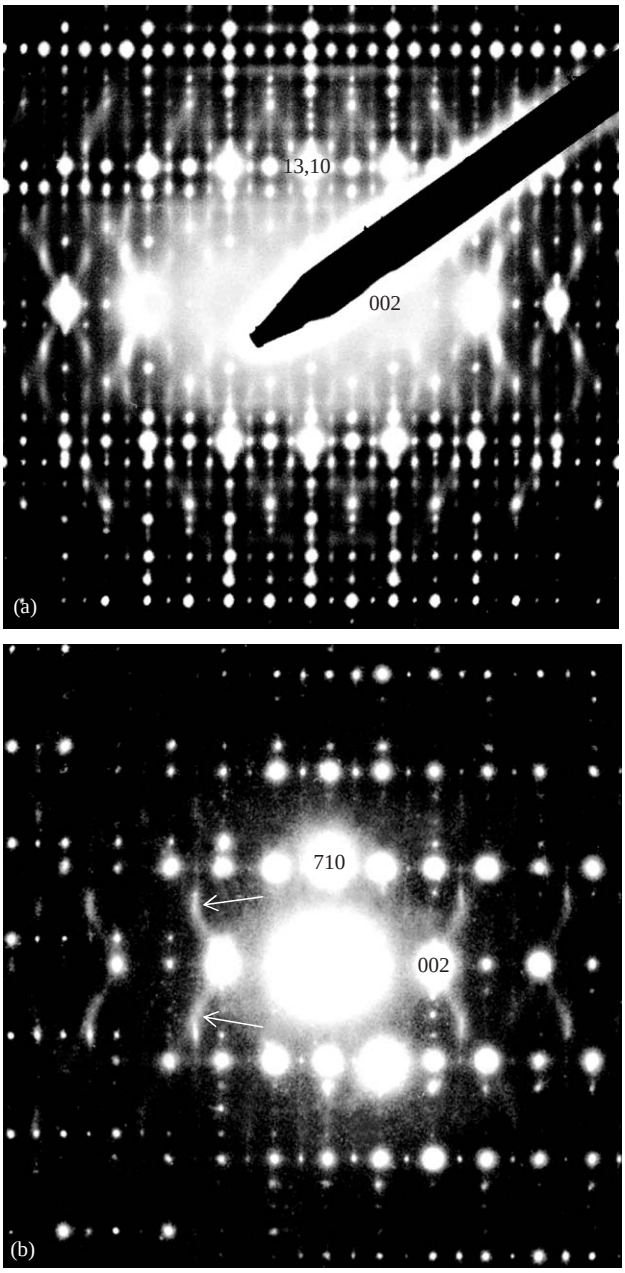

Fig. 3. (a) $\langle 1,\overline{13},0\rangle$ and (b) $\langle 1\bar{7}0\rangle$ zone axis EDPs of the room-temperature form of $AlPO_4$-8. Notice the presence of $\mathbf{G}\pm\frac{1}{2}\mathbf{c}^*$ satellite reflections as well as structured diffuse scattering (presumably corresponding to thermally excited RUM modes of distortion) in both (a) and (b).

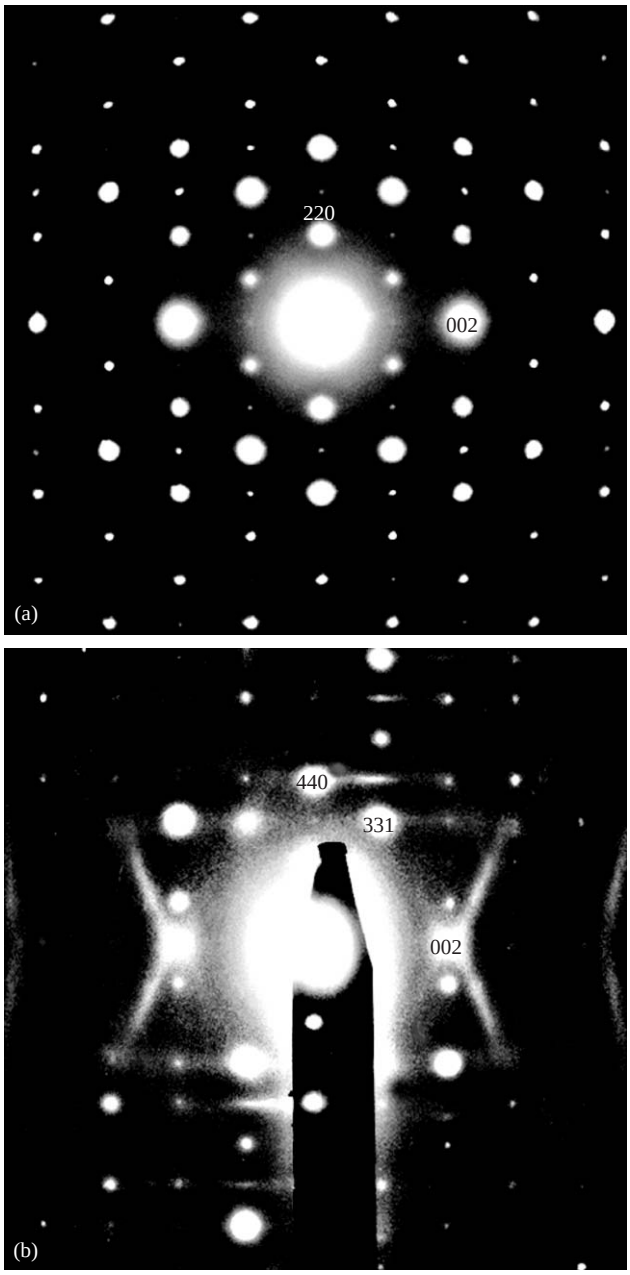

Fig. 4. (a) $\langle 110\rangle$ and (b) close to $\langle 110\rangle$ zone axis EDPs typical of the higher temperature, $Cmc2_1$ polymorphic form of $AlPO_4$-8 (induced, we believe, via beam heating). Note that the $\mathbf{G}\pm\frac{1}{2}\mathbf{c}^*$ satellite reflections have disappeared and the structured diffuse scattering in Fig. 4b running along the $\langle 331\rangle^*$ and [001]* directions of reciprocal space. This diffuse scattering is only apparent on tilting slightly away from the exact $\langle 1\bar{1}0\rangle$ zone axis orientation (see Fig. 4b) and disappears at the exact zone axis orientation (cf. Fig. 4b with Fig. 4a).

In a few grains, the $\mathbf{G}\pm\frac{1}{2}\mathbf{c}^*$ satellite reflections had disappeared suggesting a beam-induced phase transition to the higher temperature, $Cmc2_1$ polymorphic form (see Fig. 4). Structured diffuse scattering running along the $\langle 331\rangle^*$ and [001]* directions of reciprocal space were then clearly apparent on tilting slightly away from the exact $\langle 1\bar{1}0\rangle$ zone axis orientation (see Fig. 4b) but disappeared at the exact zone axis orientation (cf. Fig. 4b with Fig. 4a). This disappearance of structured diffuse scattering at an exact zone axis orientation was also characteristic of $AlPO_4$-5 as well as $AlPO_4$-11 [6,7]. Lattice dynamic calculations using the program CRUSH (see below) confirm the existence of these zero-frequency RUM modes of distortion and show that they are an intrinsic, predictable property of the tetrahedral framework structure of $AlPO_4$-8.

3.1.2. $AlPO_4$-16

Unfortunately, the grain sizes of the as-prepared $AlPO_4$-16 phase were found to be far too small to give anything other than polycrystalline ring patterns in selected-area EDPs and hence were of little use in looking for structured diffuse scattering and thereby evidence for zero-frequency RUM modes.

3.1.3. $AlPO_4$-tridymite

In the case of $AlPO_4$-tridymite, a rather complex tridymite superstructure phase was observed (see e.g. Fig. 5a) which at first glance was thought to be closely related to a known incommensurate polymorph (see Fig. 5c) of the analogous SiO_2-tridymite compound [21,34]. This incommensurate SiO_2-tridymite polymorph is characterized by incommensurate satellite reflections at $\mathbf{G} \pm m\{\frac{1}{2}[11\bar{2}0]^*_h + 0.392\mathbf{c}^*_h\}$ (where m is an integer and **G** represents a parent Bragg reflection of the underlying, originally hexagonal, tridymite parent structure—see e.g. Ref. [35]) whose intensity falls off systematically with increasing harmonic order m (see Fig. 5c). The strongest $m = 1$ primary harmonics of this incommensurate SiO_2-tridymite polymorph all fall onto a highly structured diffuse intensity distribution characteristic of the dynamically disordered high-temperature polymorphs of SiO_2-tridymite—cf., e.g., Fig. 5b with Fig. 5c; see also Refs. [34,35].

While such a hierarchical intensity distribution of the satellite reflections does not occur in Fig. 5a, there is evidence for such behaviour in the $\langle 110 \rangle_h$ (subscript h for hexagonal tridymite parent structure) zone axis EDP of this $AlPO_4$-tridymite polymorph shown in Fig. 6a. Note that the strongest satellite reflections (arrowed) in Fig. 6a fall at the $\mathbf{G} \pm \{\frac{1}{2}[\bar{1}100]^*_h + \frac{2}{5}\mathbf{c}^*_h\}$ ($\equiv \mathbf{G} \pm \{\frac{1}{2}[110]^*_h + \frac{2}{5}\mathbf{c}^*_h\}$) positions of reciprocal space. It appears that the initially incommensurate 0.392 $\mathbf{c}_h$* component has locked in to the value $\frac{2}{5}\mathbf{c}^*_h$ exactly in the case of this $AlPO_4$-tridymite polymorph. This component of the superstructure can thus be described as a locked-in RUM mode of type II (see Ref. [35]). The overall structure of this complex $AlPO_4$-tridymite polymorph, however, cannot be described as a simple locked-in variant of the incommensurate SiO_2-tridymite polymorph as there exist too many other additional satellite reflections not explained by this hypothesis as is clear from the other zone axis EDPs of this polymorph shown in Fig. 6.

Careful consideration of these EDPs shows that the observed polymorph in fact corresponds to the triclinic $F\bar{1}$ ($\mathbf{a} = 2(\mathbf{a}_h + 2\mathbf{b}_h)$, $\mathbf{b} = 2(-\mathbf{a}_h + 2\mathbf{b}_h)$, $\mathbf{c} = 10\mathbf{c}_h$; $\mathbf{a}^* = \frac{1}{4}[110]^*_h$, $\mathbf{b}^* = \frac{1}{4}[\bar{1}100]^*_h$, $\mathbf{c}^* = \frac{1}{10}[0001]^*_h$) polymorph of $AlPO_4$-tridymite whose complex crystal structure was recently successfully refined from X-ray powder diffraction data by Graetsch [23]. Indexation without the subscript h in Figs. 5a and 6 is with respect to this supercell. The appearance of this triclinic $F\bar{1}$ poly-

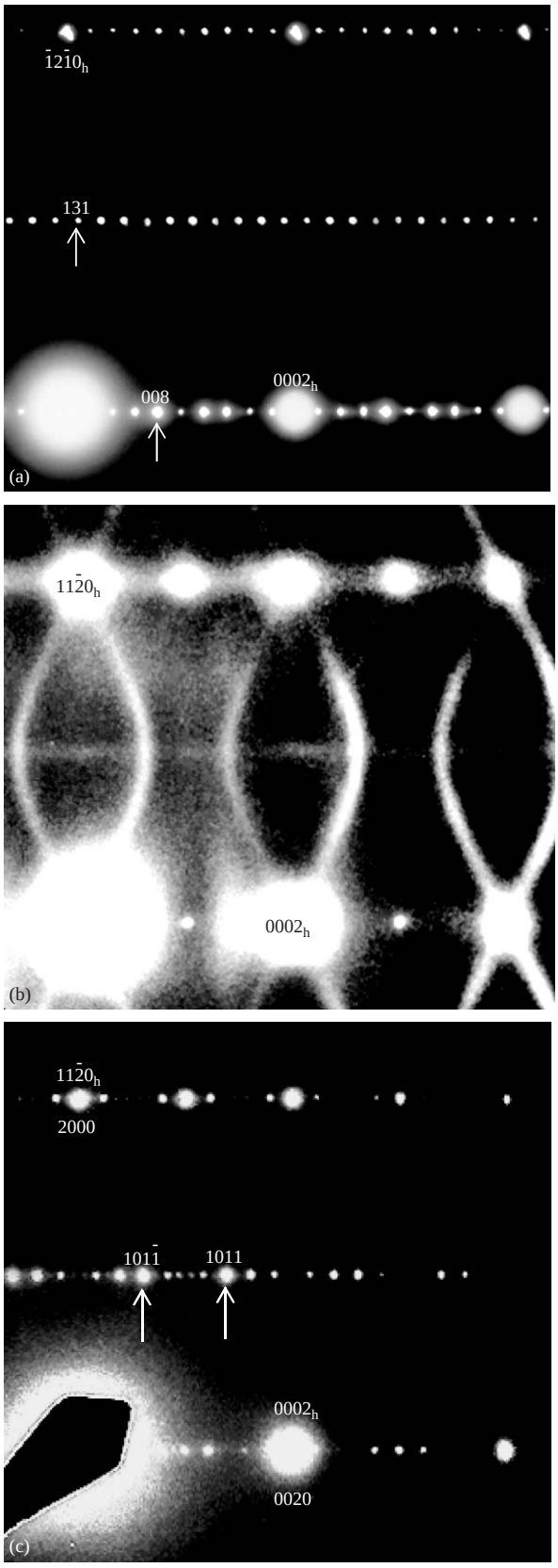

Fig. 5. $\langle \bar{1}10 \rangle_h$ (subscript h for ideal hexagonal tridymite parent structure) zone axis EDPs of (a) room-temperature $AlPO_4$-tridymite, (b) high-temperature SiO_2-tridymite and (c) an incommensurately modulated room-temperature polymorph of SiO_2-tridymite. For details see text.

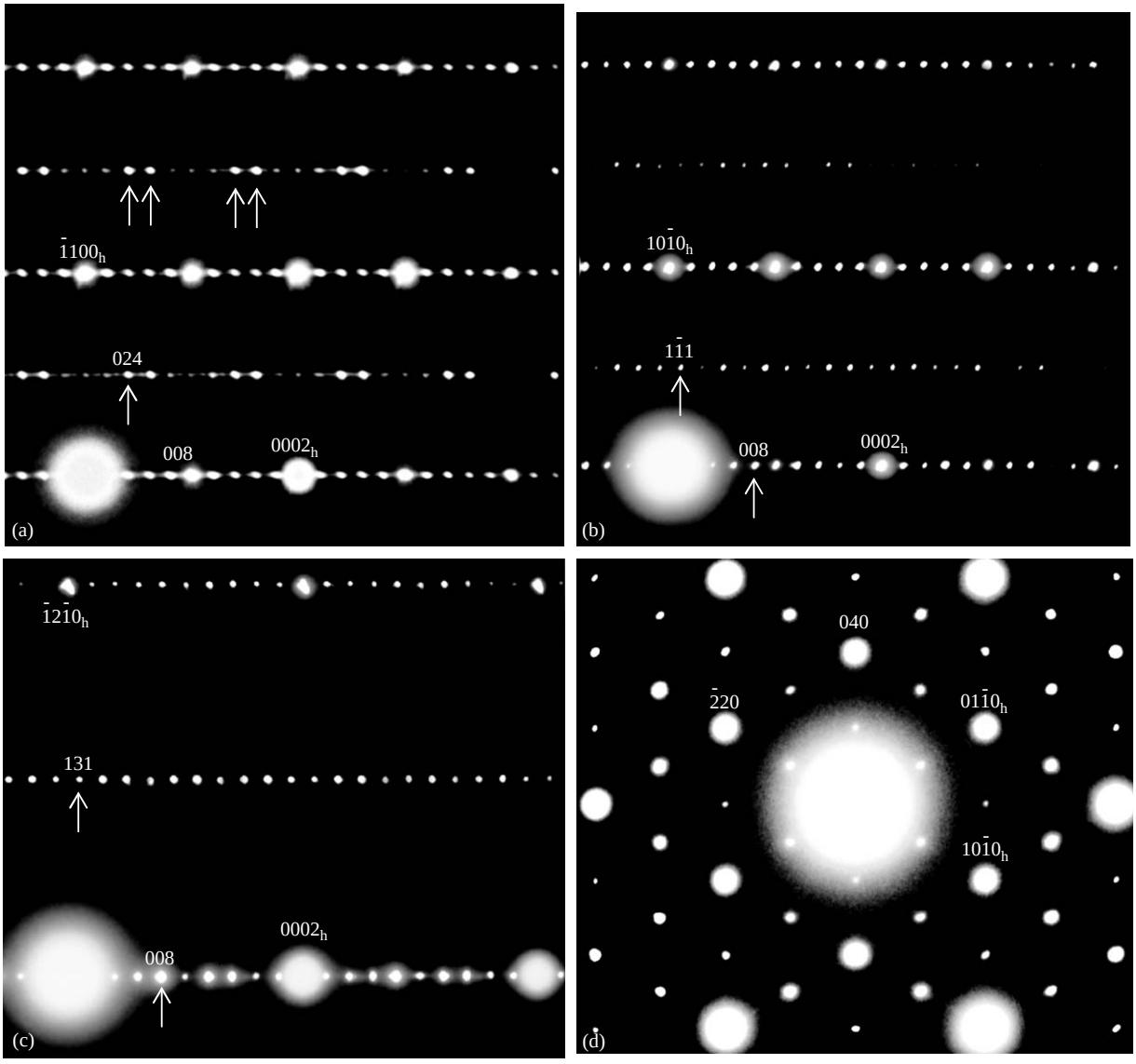

Fig. 6. (a) [100], (b) $\langle 110 \rangle$, (c) $\langle 3\bar{1}0 \rangle$ and (d) [001] zone axis EDPs of the triclinic $F\bar{1}$ ($\mathbf{a} = 2(\mathbf{a}_h + 2\mathbf{b}_h)$, $\mathbf{b} = 2(-\mathbf{a}_h + 2\mathbf{b}_h)$, $\mathbf{c} = 10\mathbf{c}_h$; $\mathbf{a}^* = \frac{1}{4}[11\bar{2}0]^*_h$, $\mathbf{b}^* = \frac{1}{4}[\bar{1}100]^*_h$, $\mathbf{c}^* = \frac{1}{10}[0001]^*_h$) polymorph of $AlPO_4$-tridymite. Indexation is given both with respect to this supercell (without the subscript h) as well as with respect to the underlying ideal hexagonal tridymite parent structure (with the subscript h in 4-index notation).

morphic form instead of the monoclinic *Pc* form suggested by XRD is attributed to the effects of grinding of the initial specimen carried out to obtain samples suitable for electron microscopy (see Ref. [23]).

In some other grains, heavy diffuse streaking along the tridymite **c*** reciprocal lattice direction occurs (see e.g. the $\langle \bar{1}10 \rangle_h$ zone axis EDP of Fig. 7). The shape (cf. Fig. 7 with Fig. 5b) and sharpness of this diffuse distribution, as well as the fact that it runs through the 0 0 0 reflection, strongly suggests that it does not arise from thermally excited RUM modes but rather arises as a result of either inherent, or grinding induced, stacking fault-type disorder on the tridymite (001) planes arising from cristobalite-type intergrowths (see e.g. Ref. [36]).

4. RUMs of the ideal $AlPO_4$-8, $AlPO_4$-16 and $AlPO_4$-tridymite structure types

The energies associated with deformation of the constituent AlO_4 and PO_4 tetrahedral units in the ideal parent structures of $AlPO_4$-8, $AlPO_4$-16 and $AlPO_4$-tridymite (see Fig. 8) are typically much larger than the energies associated with changes in their relative orientations [5–12]. Thus only RUM modes, entailing zero or minimal deformations of the essentially rigid tetrahedral units, are substantially thermally excited at elevated temperatures and thus capable of condensing out in response to lowering of temperature. The lattice dynamics program CRUSH [37] (which gives the lattice dynamical solutions to the equations of motion for a set

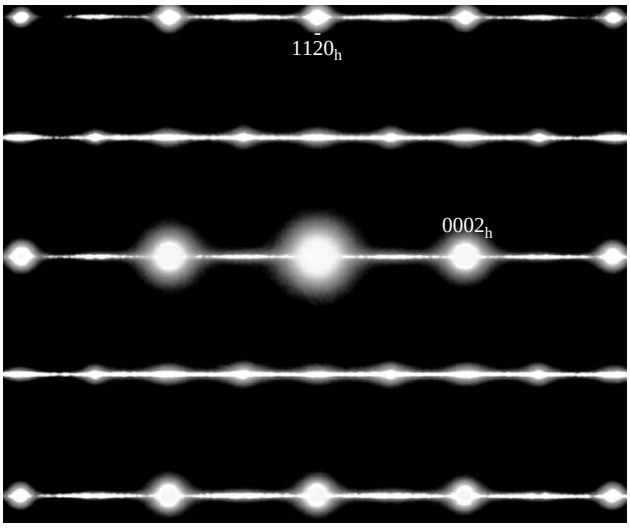

Fig. 7. Shows a $\langle \bar{1}10 \rangle_h$ zone axis EDP of a heavily stacking faulted $AlPO_4$-tridymite grain.

of linked rigid tetrahedra) has thus been used to investigate the RUM spectra of the ideal $Cmc2_1$, $AlPO_4$-8 structure type as well as that of the ideal $F23$, $AlPO_4$-16 structure type. In the case of $AlPO_4$-tridymite, the RUM spectrum of the essentially isomorphous SiO_2-tridymite is well known (see e.g. Ref. [9]) and thus does not need to be re-calculated.

4.1. $AlPO_4$-8

Given the electron diffraction results reported above and the fact that both reported structures [17,18] are already considerably distorted, the DLS constrained $Cmc2_1$ refined structures for $AlPO_4$-8 reported in Refs. [17,18] would clearly be inappropriate starting points for the purposes of the CRUSH calculation. One would like an idealized $Cmc2_1$, $AlPO_4$-8 type parent structure such that the constituent AlO_4 and PO_4 tetrahedra are each regular and of the correct size [8–12,37]. Given the relatively low average structure space group symmetry, the average structure unit cell dimensions and the complexity of the tetrahedral connectivity (see Fig. 8a and b), this is a distinctly non-trivial task. Instead, a somewhat idealized version of the average *Cmcm* structure of $AlPO_4$-8 refined by Richardson and Vogt [19] was deemed to be the most appropriate starting point (see Table 2 and Fig. 8a and b). Note that average *Cmcm* symmetry means that this structure does not distinguish between AlO_4 and PO_4 tetrahedra. For the purposes of the CRUSH calculation, however, this makes very little difference.

With this idealized parent structure, six zero-frequency RUM modes of distortion were thereby predicted to exist for a general modulation wave-vector of the form $\mathbf{q} = \gamma \mathbf{c}^*$ with this number rising to $(6+2) = 8$

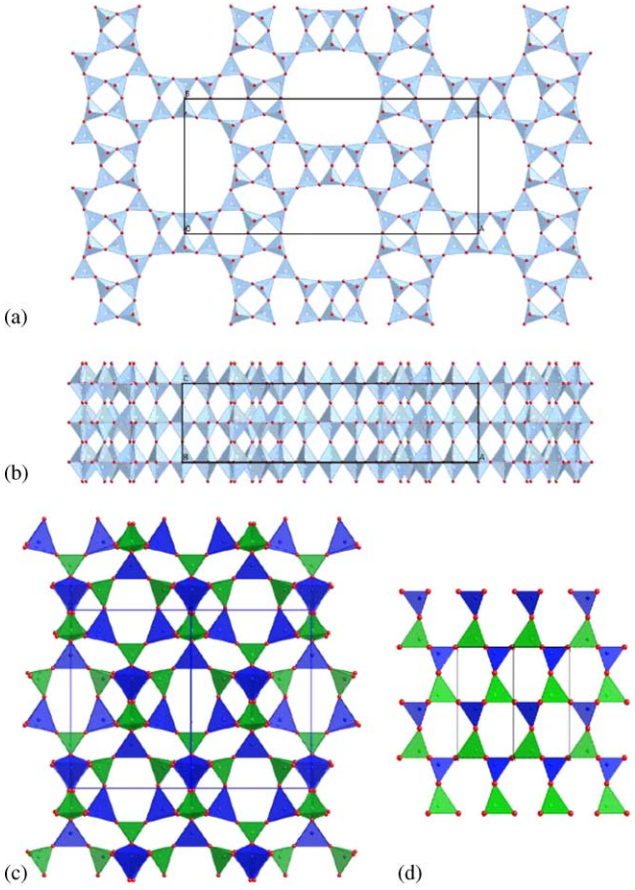

Fig. 8. Idealized *Cmcm* parent structure of $AlPO_4$-8 (see Table 2) in projection down [001] in (a) and [010] in (b). In *Cmcm* the AlO_4 and PO_4 tetrahedra are not distinguished and hence they are shown as light blue. (c) Refined $F23$ structure of $AlPO_4$-16 in projection down $\langle 110 \rangle$ while (d) shows the ideal highest hexagonal polymorph of $AlPO_4$-tridymite in projection down $\langle 110 \rangle$. The AlO_4 tetrahedra are dark blue in (c) and (d) while the PO_4 tetrahedra are shown in green.

RUM modes of distortion for the wave-vector magnitude $\gamma = \frac{1}{2}$. Experimentally, little evidence for diffuse streaking along $\mathbf{c}^*$ could be found in the doubled $\mathbf{c}$-axis, room-temperature polymorphic form (see e.g. Fig. 3). On the other hand, considerable diffuse streaking along $\mathbf{c}^*$ is apparent in the higher-temperature $Cmc2_1$ polymorphic form (see Fig. 4b). This strongly suggests that the $\mathbf{q} = \frac{1}{2}\mathbf{c}^*$ mode responsible for the phase transition from the high-temperature to room-temperature polymorphic forms corresponds to a condensed $\mathbf{q} = \frac{1}{2}\mathbf{c}^*$ RUM mode. The freezing out of this particular RUM mode appears to lead to the disappearance of the other $\mathbf{q} = \gamma \mathbf{c}^*$ RUM modes (cf. Fig. 4b with Fig. 3). Unfortunately, the CRUSH-derived RUM eigenvectors associated with the $\gamma = \frac{1}{2}$ point are extremely complex and were not able to be simply interpreted.

With the above idealized parent structure, some 18 RUM modes of distortion were also predicted to exist for any $\mathbf{q} = [hk0]^*$ modulation wave-vector.

Table 2
Idealized fractional coordinates of $AlPO_4$-8 (space group symmetry $Cmc2_1$) used for the purposes of the CRUSH calculation (T: Al or P) along with those reported in Ref. [19]

Atom	Ideal ($a = 33.2900$ Å, $b = 14.7036$ Å, $c = 8.3863$ Å)			Richardson and Vogt [19] ($a = 33.2900$ Å, $b = 14.7040$ Å, $c = 8.3860$ Å)		
	x	y	z	x	y	z
T 1	0.1862	0.3999	0.0647	0.1904	0.4160	0.0660
T 2	0.0000	0.0958	0.9356	0.0000	0.1320	0.9720
T 3	0.0819	0.1030	0.0637	0.0878	0.0940	0.0550
T 4	0.2723	0.4016	0.9351	0.2740	0.4040	0.9390
T 5	0.1564	0.2201	0.9352	0.1573	0.2260	0.9290
O 1	0.1725	0.5000	0.0000	0.1767	0.5000	0.0000
O 2	0.0000	0.0000	0.0000	0.0000	0.0000	0.0000
O 3	0.1862	0.3999	0.2500	0.1772	0.4020	0.2500
O 4	0.0000	0.0958	0.7500	0.0000	0.1270	0.7500
O 5	0.0404	0.1437	0.0000	0.0456	0.1330	0.0180
O 6	0.2297	0.3771	0.0000	0.2317	0.3940	0.0200
O 7	0.1563	0.3227	0.0000	0.1580	0.3240	0.0310
O 8	0.1954	0.1722	0.0000	0.1993	0.1750	0.0170
O 9	0.0876	0.0000	0.0000	0.0906	0.0000	0.0000
O 10	0.0819	0.1030	0.2500	0.0847	0.0960	0.2500
O 11	0.2732	0.4016	0.7500	0.2590	0.3780	0.7500
O 12	0.1564	0.2201	0.7500	0.1444	0.2320	0.7500
O 13	0.1176	0.1653	0.0000	0.1154	0.1740	0.0020
O 14	0.2852	0.5000	0.0000	0.2865	0.5000	0.0000

Experimentally, $[hk0]^*$ diffuse streaking is not particularly apparent although remnants thereof are apparent in Figs. 3 and 4b in addition to a more curved (hyperbolic) type of diffuse distribution. Note that this more general (hyperbolic) type of diffuse distribution is quite close to running along the $\langle 331 \rangle^*$ directions of reciprocal space in the close to $\langle 110 \rangle$ zone axis EDP of Fig. 4b. To confirm that this type of diffuse streaking arises from thermally excited RUM modes, the zero-frequency RUM modes of distortion in the $\{hhl\}^*$ planes of reciprocal space have also been calculated (see Fig. 9). Such calculations indeed show the existence of zero-frequency RUM modes of distortion running along the $\langle 331 \rangle^*$ directions of reciprocal space. Note that the curves shown in Fig. 9 must repeat with the reciprocal space periodicity of the parent reciprocal lattice. Only some of these symmetry-related curves have been shown in Fig. 9 to facilitate easier comparison with the experimental EDP shown in Fig. 4b. Thus RUMs do indeed appear to exist for each point on the experimentally observed diffuse distribution.

Further progress requires a total scattering investigation [12,38,39] of $AlPO_4$-8 including both Bragg scattering as well as the structured diffuse scattering characteristic of this framework topology.

4.2. $AlPO_4$-16

Given the poor crystal chemistry of the reported $F23$ average structure of $AlPO_4$-16 [16] (see Table 1), it would clearly be an inappropriate starting point for the purposes of the CRUSH calculation. Instead, an idealized $Fm\bar{3}m$, SiO_2 (or high-temperature octadecasil—see Ref. [40]) type parent structure has been derived (see Table 3) such that the constituent $(Al,P)O_4$ tetrahedra are each identical and of the correct (SiO_4) tetrahedral size [8–12,37]. Note that average $F23$ space group symmetry goes to average $Fm\bar{3}m$ symmetry when the distinction between AlO_4 and PO_4 tetrahedra is removed. The idealized structure of Table 3 does not distinguish between AlO_4 and PO_4 tetrahedra. For the purposes of the CRUSH calculation, however, this makes very little difference.

Without the guidance of experimental EDPs, it is difficult to know along which direction/s of reciprocal space to look for RUM modes. We have therefore only investigated the $\langle 001 \rangle^*$ and $\langle hk0 \rangle^*$ directions of reciprocal space. Fourteen zero-frequency RUM modes were predicted to exist for a general $\mathbf{q} = \gamma\langle 001 \rangle^*$ modulation wave-vector with this number rising to 22, made up of 19 RUM modes plus 3 acoustic modes, for the special zone centre wave-vector magnitude $\gamma = 0.12$ zero-frequency RUM modes were predicted to exist for a general $\mathbf{q} = \gamma\langle hk0 \rangle^*$ modulation wave-vector. Clearly, in the case of $AlPO_4$-16, there is plenty of scope for dynamically excited RUM modes.

It is of interest to note that a condensed $\mathbf{q} = \mathbf{0}$ RUM mode is clearly responsible for the $Fm\bar{3}m$ ($\mathbf{a}_p$, $\mathbf{b}_p$, $\mathbf{c}_p$) to $I4/m(\mathbf{a} = \frac{1}{2}(\mathbf{a}_p - \mathbf{b}_p)$, $\mathbf{b} = \frac{1}{2}(\mathbf{a}_p + \mathbf{b}_p)$, $\mathbf{c} = \mathbf{c}_p)$ phase transition recently observed to occur in dehydrated SiO_2 octadecasil (i.e. the all SiO_2 analogue of $AlPO_4$-16) at $\sim$500 °C [40] (see Fig. 10). Fig. 10a shows the rotations

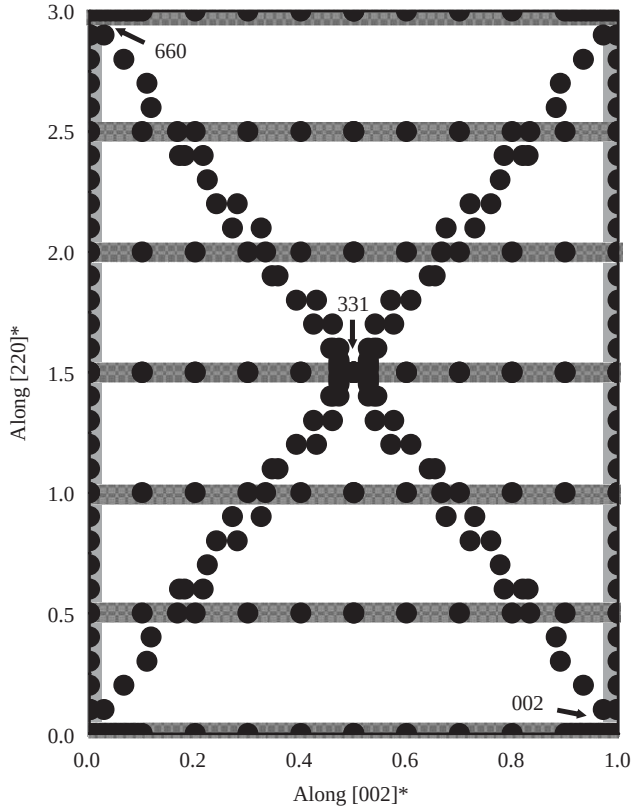

Fig. 9. Calculated RUM modes of distortion of the idealized *Cmcm* parent structure of $AlPO_4$-8 (see Table 2) in a $\langle hhl \rangle^*$ section of reciprocal space for comparison with Fig. 4b. Individual RUM mode wave-vectors are shown with large dots while the grey lines represent 'soft' directions of reciprocal space. Note that the curves shown must repeat with the reciprocal space periodicity of the parent reciprocal lattice. Only some of these symmetry-related curves have been shown in Fig. 9 to facilitate easier comparison with Fig. 4b.

Table 3
Idealized fractional coordinates of SiO_2 (of $AlPO_4$-16 structure type) used for the purposes of the CRUSH calculation (*T*: Al or P)

Atom	Ideal ($Fm\bar{3}m$, $a = 13.7517$ Å)		
	x	*y*	*z*
T 1	0.1136	0.1136	0.1136
T 2	0.7500	0.2500	0.2500
O 1	0.0000	0.1364	0.1364
O 2	0.1818	0.1818	0.1818

around [001] that are needed to transform the high-temperature cubic form into the lower-temperature tetragonal form shown in Fig. 10b. Note that such a RUM mode could, in principle, equally well occur around any one of the three originally equivalent $\langle 001 \rangle$ directions (or any combination thereof) and hence this particular 'soft' RUM mode is triply degenerate in the 'disordered' high-temperature form. The authors of Ref. [40] suggest that cubic symmetry in both SiO_2 octadecasil and $AlPO_4$-16

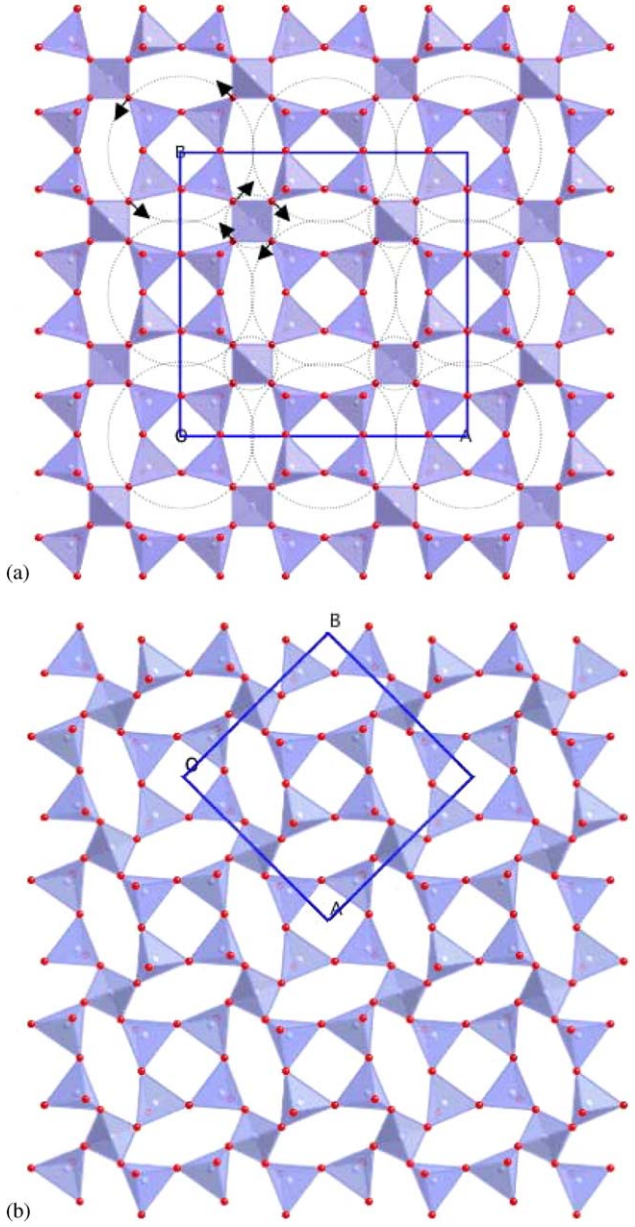

Fig. 10. (a) RUM rotations around [001] that are needed to transform the high-temperature $Fm\bar{3}m$ ($\mathbf{a}_p$, $\mathbf{b}_p$, $\mathbf{c}_p$) cubic form of dehydrated SiO_2 octadecasil (the all SiO_2 analogue of $AlPO_4$-16) into the lower-temperature $I4/m$ ($\mathbf{a} = \frac{1}{2}(\mathbf{a}_p - \mathbf{b}_p)$, $\mathbf{b} = \frac{1}{2}(\mathbf{a}_p + \mathbf{b}_p)$, $\mathbf{c} = \mathbf{c}_p$) tetragonal shown in (b).

arises only from '…the presence of structural defects (and) is likely responsible for the symmetry change …'. We believe, however, that cubic symmetry does not arise from structural defects but rather from the simultaneous dynamic excitation of RUM modes.

5. Conclusions

Clearly, all three $AlPO_4$ compounds investigated show direct evidence for thermally excited RUM modes

of distortion at high temperature, any one of which (or any combination of which) could potentially condense out at lower temperature/s giving rise to extremely complex lower-temperature polymorphism, as e.g., in the case of $AlPO_4$-tridymite. In the case of $AlPO_4$-8, one such condensed $\mathbf{q} = \frac{1}{2}\mathbf{c}^*$ RUM mode has clearly condensed out at room temperature. Only total scattering studies including both Bragg reflections as well as the underlying diffuse scattering can hope to unravel the structural complexities of these fascinating zeotypic microporous aluminophosphate phases.

References

[1] S.T. Wilson, B.M. Lok, C.A. Messina, T.R. Cannan, E.M. Flanigen, J. Am. Chem. Soc. 104 (1982) 1146–1147.
[2] E.M. Flanigen, B.M. Lok, R.L. Patton, S.T. Wilson, Pure Appl. Chem. 58 (1986) 1351–1358.
[3] E.M. Flanigen, R.L. Patton, S.T. Wilson, Stud. Surf. Sci. Catal. 37 (1988) 13–27.
[4] D.B. Akolekar, J. Mol. Catal. A: Chem. 104 (1995) 95–102.
[5] P. Demontis, J. Gulín González, G.B. Suffriti, A. Tilocca, C. de las Pozas, Micropor. Mesopor. Mater. 42 (2001) 103–111.
[6] Y. Liu, R.L. Withers, L. Norén, Solid State Sci. 5 (2003) 427–434.
[7] Y. Liu, R.L. Withers, J. Solid State Chem. 172 (2003) 431–437.
[8] K.D. Hammonds, M.T. Dove, A.P. Giddy, V. Heine, B. Winkler, Am. Miner. 81 (1996) 1057–1079.
[9] M.T. Dove, A.K.A. Pryde, D.A. Keen, Miner. Mag. 64 (2000) 267–283.
[10] R.L. Withers, Solid State Sci. 5 (2003) 115–123.
[11] M.T. Dove, V. Heine, K.D. Hammonds, M. Gambhir, A.K.A. Pryde, Short range disorder and long range order: implications of the Rigid Unit Mode model, in: S.J.L. Billinge, M.F. Thorpe (Eds.), Local Structure From Diffraction, Plenum Press, New York, 1998, pp. 253–271.
[12] M.G. Tucker, M.T. Dove, D.A. Keen, Total scattering and reverse monte carlo modelling of disordered crystalline materials, in: S.J.L. Billinge, M.F. Thorpe (Eds.), From Semiconductors to Proteins, Kluwer Academic/Plenum Publishers, New York, 2002, pp. 105–128.
[13] J.M. Bennett, J.W. Richardson, J.J. Pluth, J.V. Smith, Zeolites 7 (1987) 160–162.
[14] S. Qiu, Q. Pang, H. Kessler, J.L. Guth, Zeolites 8 (1989) 440–444.
[15] N.E. Brese, M. O'Keeffe, Acta Crystallogr. B 47 (1991) 192–197.
[16] J.M. Bennett, R.M. Kirchner, Zeolites 11 (1991) 502–506.
[17] R.M. Dessau, J.L. Schlenker, J.B. Higgins, Zeolites 10 (1990) 522–524.
[18] M.D. Poojary, A. Clearfield, Mater. Chem. Phys. 35 (1993) 301–304.
[19] J.W. Richardson, E.T.C. Vogt, Zeolites 12 (1992) 13–19.
[20] H. Graetsch, O.W. Flörke, Z. Krist. 195 (1991) 31–48.
[21] R.L. Withers, J.G. Thompson, Y. Xiao, R.J. Kirkpatrick, Phys. Chem. Miner. 21 (1994) 421–433.
[22] M. Spiegel, W. Hoffmann, J. Löns, Eur. J. Miner. 2 (1990) 246–255.
[23] H. Graetsch, Acta Crystallogr. C 56 (2003) 401–403.
[24] H. Graetsch, Acta Crystallogr. C 58 (2002) i18–i20.
[25] Z. Liu, N. Fujita, O. Terasaki, T. Ohsuna, K. Hiraga, M.A. Camblor, M.-J. Díaz-Cabanas, A.K. Cheetham, Chem. Eur. J. 8 (2002) 4549–4556.
[26] M.E. Davis, C. Saldarriaga, C. Montes, J. Garces, C. Crowder, Nature 331 (1988) 698–701.
[27] J.W. Richardson, J.V. Smith, J.J. Pluth, J. Phys. Chem. 93 (1989) 8212–8219.
[28] J. Patarin, C. Schott-Darie, P.Y. Le. Goff, H. Kessler, E. Benazzi, Stud. Surf. Sci. Catal. 98 (1995) 256–257.
[29] SRM 640c, National Institute of Standards and Technology, 13/9, 2000.
[30] B. Noläng, Department of Materials Chemistry, Ångstömlaboratoriet, S-752 21 Uppsala, Sweden.
[31] N.J. Henson, A.K. Cheetham, J.D. Gale, Chem. Mater. 8 (1996) 664–670.
[32] E. de Vos Burchart, H. van Bekkum, B. de Graaf, E.T.C. Vogt, J. Chem. Soc. Faraday Trans. 88 (1992) 2761–2769.
[33] http://www.cryst.ehu.es/cryst/maxsub.html;
See also E. Kroumova, M.I. Aroyo, J.M. Perez Mato, A. Kirov, C. Capillas, S. Ivantchev, H. Wondratschek, Phase Trans. 76 (2003) 155–170.
[34] R.L. Withers, Solid State Sci. 5 (2003) 115–123.
[35] Ray L. Withers, Y. Liu, in: G. Meyer, D. Naumann, L. Wesemann (Eds.), Inorganic Chemistry in Focus II, Wiley-VCH, Weinheim, 2005, pp. 347–363.
[36] H. Lemmens, M. Czank, G. van Tendeloo, S. Amelinckx, Phys. Chem. Miner. 27 (2000) 386–397.
[37] K.D. Hammonds, M.T. Dove, A.P. Giddy, V. Heine, Am. Miner. 79 (1994) 1207–1209.
[38] M.G. Tucker, M.P. Squires, M.T. Dove, D.A. Keen, J. Phys. Cond. Matt. 13 (2001) 403–423.
[39] D.A. Keen, M.T. Dove, Miner. Mag. 64 (2000) 447–457.
[40] L.A. Villaescusa, P.A. Barrett, M.A. Camblor, Chem. Mater. 10 (1998) 3966–3973.